Mathematical and Computational Applications, Vol. 9, No. 3, pp. 333-347, 2004.

ON THE MATHEMATICAL MODELLING OF BEAMS ROTATING ABOUT A FIXED AXIS

Sevda Telli and Osman Kopmaz
Dept. of Mechanical Engineering, College of Engineering and Architecture
Uludag University, Gorukle, Bursa 16059, Turkey
okopmaz@uludag.edu.tr

Abstract- In this paper, the equations of motion of a rotating beam encountered in various mechanical systems are given in the Euler-Newtoian form using four different dynamic modelling approaches. These models differ from each other in that they use different elastic displacements to define the state of deformed beam, i.e. the longitudinal and transversal deflections model, the axial and transversal deflections model, the axial, transversal deflections and slope angle model, and finally the transversal deflection with normal force model, which are abbreviatedly denoted by the UVM, the SVM, the SVφM, and the VNM. Following a brief discussion about geometric relationship among three linear elastic displacements,–that is, the longitudinal *u*-, the transversal *v*-, and the axial *s*-displacements– geometric stiffening effect, and the choice of spatial functions consistent with boundary conditions to discretize equations of motion, simulation results found from these models are presented in graphics, and comparatively evaluated. It is concluded that the SVM and the SVφM is most reliable models provided that the comparison functions for axial displacement *s* are the eigenmodes of a fixed-free, longitudinally vibrating rod. The VNM appears to be a prudential model, because it always gives results above those obtained by the SVM.

Keywords- Flexible Link, Rotating Flexible Beam, Vibration of Elastic Systems

1. INTRODUCTION

Most engineering applications include flexible bodies rotating about a fixed or moving axis in space such as robot arms, hard disc drivers, solar panel carriers or antennas of satellites, and helicopter blades, which operate at very high speeds. Thus, they may considerably deform so that the whole system cannot function properly or may sometimes fails completely. In this regard, accurate modelling and analysis of mechanical systems or their critical parts have become indispensable. There has been very intensive work on the subject in last two decades under the headline "rotating beam dynamics" which can be classified into two main groups. The first group of papers deals with the motion control of flexible beams using simple dynamic models because they operates at speeds lower than first natural frequency [1,2,3,4] while the other group of papers concentrates on developing possibly accurate and realistic dynamic models [5-14]. Among them, there are a few detailed treatments on modelling of flexible single or multibody system [9,12,14]. The use of a rotating coordinate system attached to the undeformed imaginary beam is a common practice for many authors. To define the deformed position of a rotating beam two of three elastic displacements, i.e. the transversal, the longitudinal and the axial displacements, which are usually denoted by

v, u and s, can be employed. Since the equations of motion are generally non-linear and coupled they can be solved by discretization. Hence, the appropriate choice of comparison functions is significant. Another point to be considered in the modelling of rotating bodies is the geometric stiffening due to centrifugal forces. Although these two issues are well known by relevant research community, some principal errors are observed in the literature if rarely. For instance, in [12] the same set of generalized coordinates are used for all elastic displacements. In the models proposed in [13] geometric stiffening terms do not appear in the equations derived. Furthermore, a comparative study regarding dynamic models used so far has not published yet, to the authors' knowledge. The present paper primarily aims to compare and discuss different models used for dynamic analysis of a rotating beam. To this end, first the relationship among there elastic displacements will be given and discussed. Then the results of simulations made by a MATLAB code will be presented in graphics and evaluated.

2. EQUATIONS OF MOTION

Consider a beam rotating about z-axis as shown in Figure 1. It is assumed that the beam is homogenous and uniform. Its length, cross-sectional area, second moment of area, density and Young modulus are L, A, I, ρ, and E, respectively. θ is the rotation angle of the beam measured from a fixed frame. Its first and second derivatives with respect to time, i.e. $\dot{\theta}$ and $\ddot{\theta}$ are the angular speed and acceleration of the beam. Time derivatives are denoted by dots over the letters.

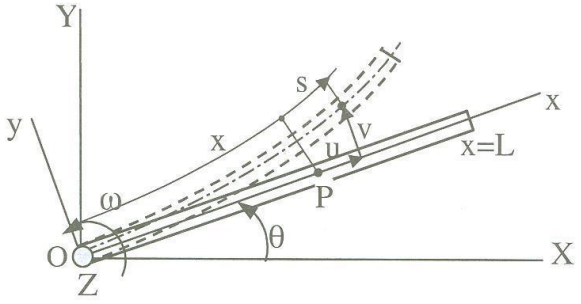

Figure 1. Rotating beam in its deformed position.

The motion is assumed to occur in the horizontal plane, so that the potential of beam weight can be disregarded. In the study of motion a rotating coordinate system xOy will be used. The XOY-system is a fixed coordinate system. At any time t, the linear relative displacement of a generic point P which is initially at x on the beam can be decomposed into two components u and v along x and y axes, respectively, which are called longitudinal and transversal elastic displacements as referred to the undeformed state of beam. However, the axial elastic displacement s can also be used in the equations of motion instead of u. The axial displacement s is measured on the median line of the deformed beam. The differential relationship among these three elastic displacements is as follows:

$$(ds+dx)^2=\left[(dx+du)^2+dv^2\right] \tag{1}$$

or in the derivative form

$$\left(1+\frac{\partial s}{\partial x}\right)=\left[\left(1+\frac{\partial u}{\partial x}\right)^2+\left(\frac{\partial v}{\partial x}\right)^2\right]^{1/2} \tag{2}$$

The rhs of equations (2) is usually expanded into a binomial series, and one holds up to the first three terms. Thus, the following approximation is obtained:

$$\frac{\partial s}{\partial x}=\frac{\partial u}{\partial x}+\frac{1}{2}\left(\frac{\partial v}{\partial x}\right)^2 \tag{3}$$

If the shear force effect is to be included in models then the number of elastic coordinates will be five, i.e., u, v, s, φ and γ. Here φ and γ are bending rotation and shear angle, respectively. It is well known that there is also a relation among v, φ and γ, as follows:

$$\frac{dv}{dx}=\varphi+\gamma \tag{4}$$

There are five elastic coordinates against two relationships (equations (2) and (4)). Hence, three of them can be selected main dependent variables. The parameter that describes the rigid body motion of beam is θ. Assume that the actuator has such a torque characteristic that a desired motion program $\theta(t)$ can be provided. Then, to obtain only the equations of motion associated with u, v, φ or s, v, φ will be sufficient.

The conventional procedure to derive the Lagrangean equations of motion will not be given here. The coupled equations of motion related to u, v and φ are obtained as

$$\ddot{u}-u\dot{\theta}^2-2\dot{v}\dot{\theta}-v\ddot{\theta}-\frac{E}{\rho}\left(u'+\frac{1}{2}v'^2\right)'=x\dot{\theta}^2 \tag{5}$$

$$\ddot{v}+2\dot{u}\dot{\theta}-v\dot{\theta}^2+u\ddot{\theta}-k'\frac{G}{\rho}(v''-\varphi')-\frac{E}{\rho}\left[\left(u'+\frac{1}{2}v'^2\right)v'\right]'=-x\ddot{\theta} \tag{6}$$

$$\ddot{\varphi}-\frac{E}{\rho}\varphi''-k'\frac{GA}{\rho I}(v'-\varphi)=-\ddot{\theta} \tag{7}$$

while those related to s, v and φ are as follows:

$$\left(s-\frac{1}{2}\int_0^x v'^2dx\right)^{\bullet\bullet}-\dot{\theta}^2\left(s-\frac{1}{2}\int_0^x v'^2dx\right)-2\dot{\theta}\dot{v}-\ddot{\theta}v-\frac{E}{\rho}s''=\dot{\theta}^2x \tag{8}$$

$$\ddot{v}+2\dot{\theta}\left(s-\frac{1}{2}\int_0^x v'^2dx\right)^{\bullet}-v\dot{\theta}^2+\left(s-\frac{1}{2}\int_0^x v'^2dx\right)\ddot{\theta}-k'\frac{G}{\rho}\left(v''-\varphi'\right)-\frac{E}{\rho}\left(s'v'\right)'=-x\ddot{\theta} \tag{9}$$

$$\ddot{\varphi}-\frac{E}{\rho}\varphi''-k'\frac{GA}{\rho I}(v'-\varphi)=-\ddot{\theta} \tag{10}$$

where the dots and primes over letters, parentheses or brackets, denote the derivations with respect to time t and position x, respectively. Since bending moment has more

dominant effect on the transversal deflections than that of shear force for long beams, it will be useful to re-derive the equations (5 to 7) and (8 to 10) assuming that $\varphi \cong v'$. Thus, the equations related to u and v become as follows:

$$\ddot{u} - u\dot{\theta}^2 - 2\dot{v}\dot{\theta} - v\ddot{\theta} - \frac{E}{\rho}\left(u' + \frac{1}{2}v'^2\right)' = x\dot{\theta}^2 \tag{11}$$

$$\ddot{v} + 2\dot{u}\dot{\theta} - v\dot{\theta}^2 + u\ddot{\theta} + \frac{EI}{\rho A}v'''' - \frac{I_{zz}}{A}\ddot{v}'' - \frac{E}{\rho}\left[\left(u' + \frac{1}{2}v'^2\right)v'\right]' = -x\ddot{\theta} \tag{12}$$

while those in s and v are found as :

$$\left(s - \frac{1}{2}\int_0^x v'^2 dx\right)^{\bullet\bullet} - \dot{\theta}^2\left(s - \frac{1}{2}\int_0^x v'^2 dx\right) - 2\dot{\theta}\dot{v} - \ddot{\theta}v - \frac{E}{\rho}s'' = \dot{\theta}^2 x \tag{13}$$

$$\ddot{v} + 2\dot{\theta}\left(s - \frac{1}{2}\int_0^x v'^2 dx\right)^{\bullet} - v\dot{\theta}^2 + \left(s - \frac{1}{2}\int_0^x v'^2 dx\right)\ddot{\theta} + \frac{EI}{\rho A}v'''' - \frac{I_{zz}}{A}\ddot{v}'' - \frac{E}{\rho}\left(s'v'\right)' = -x\ddot{\theta} \tag{14}$$

The effect of rotatory inertia can be abandoned by dropping the term $(I_{zz}/A)\ddot{v}''$ in equations (12 and 14). Henceforth, the model given by equations (11-12) will be called the (u-v)-model or the UVM, the model based on equations (8 to 10) the (s-v-φ)-model or the SVφM, and finally, that of equations (13-14) the (s-v)-model or the SVM. It is observed that equations (13) and (14) can be simply obtained by replacing the terms related to u and their derivatives in equations (11) and (12) with its counterpart given by equation (3). Some authors use only one equation of motion for transversal vibrations in the form of

$$\ddot{v} - v\dot{\theta}^2 + \frac{EI}{\rho A}v'''' - \frac{I}{A}\ddot{v}'' - \left(N v'\right)' = -x\ddot{\theta} \tag{15}$$

instead of the coupled (u-v)-model [6]. In order to take the geometric stiffening effect into account, the transversal component of the normal force included by rotation is included in equation (15) via the term $(Nv')'$. The counterpart of this term in the (u-v)-model is $EA\left(u' + v'^2/2\right)$. Note that the coefficient of the term in equation (11) is E/ρ but not EA, because all the terms of that equation are divided by ρA. Since the u deflections are assumed to be very small under the practical operating conditions, the normal force N in equation (15) is sometimes replaced with the centrifugal inertia force for undeflected beam, which will be denoted by N_M, as follows:

$$N_M = \frac{1}{2}\rho A\dot{\theta}^2\left(L^2 - x^2\right) \tag{16}$$

In the following sections of the paper, this model also will be called the (v-N)-model or the VNM.

Before the presentation of numerical results some terms in the equations of motion will be briefly discussed because they determine whether numerical solutions diverge or not. The term of $-v\dot{\theta}^2$ appearing in equations (6), (9), (12), (14) and (15) represents the so-called geometric softening. This term causes the divergence of solution at the angular

speeds higher than the first bending frequency which can be differ from each other depending on comparison/admissible function chosen. Whichever method is used, either the Galerkin or the assumed modes method, this is the case. On the contrary, the term

$-\frac{E}{\rho}\left[\left(u'+\frac{1}{2}v'^2\right)v'\right]'$ in equations (6) and (12), and the term

$-\frac{E}{\rho}\left(s'v'\right)'$ in equations (9) and (14) present the geometric stiffening, and ensure the convergence of numeric solutions. Another noteworthy point that the system becomes stiffer in the mathematical sense when the modal functions of a fixed-free longitudinal vibrating rod are used as shape functions for u in equations (11) and (12). Thus, the deflections u and v smaller than that of they must be are obtained.

The equations of motion associated with the SVM, UVM, SVφM and VNM were re-derived using the assumed modes method. The sets of coupled, ordinary differential equations obtained were solved by means of an odesolver ODE15s that is also suitable for stiff equations and a built-in code in MATLAB

To make a comparison among the models presented so far with regard to their range of validity and the order of results produced by them simulations were carried out choosing a specific program for $\dot{\theta}(t)$ which is also used in [9,12,14]. The coming section will be devoted to the presentation, comparison and discussion of numerical results.

3. NUMERIC RESULTS AND DISCUSSION

The simulations were carried out based on a cycloidal time function for angular speed ω in the following form:

$$\begin{aligned} \omega = \dot{\theta} &= \omega_0\left(\frac{t}{T}-\frac{1}{2\pi}\sin\frac{2\pi t}{T}\right) && 0\le t\le T \\ \omega &= \omega_0 && t>T \end{aligned} \qquad (17)$$

where ω_0 denotes the maximum angular speed of beam when $t \geq T$. Then, the angular acceleration α varies as follows:

$$\begin{aligned} \alpha = \ddot{\theta} &= \frac{\omega_0}{T}\left(1-\cos\frac{2\pi t}{T}\right) && 0\le t\le T \\ \alpha &= 0 && t>T \end{aligned} \qquad (18)$$

The graphics of ω and α are plotted in Figure 2a and b. The magnitude of angular acceleration causing transversal deflections is determined by two parameters, i.e. ω_0 and T while, on the other hand, the angular speed given by (17) is the only source of geometric stiffening. Either kinematic entity affect the dynamic behaviour of beam oppositely. It is obvious from (18) that increasing T for a fixed ω_0 reduces angular

acceleration which leads to a decrease in transversal displacements. At first glance, it can be thought that same transversal deflections would occur as long as the ratio of ω_0/T

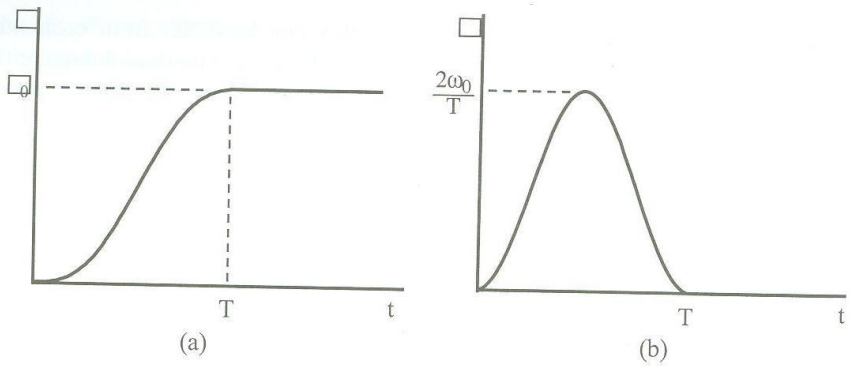

Figure 2. Variation of **a)** angular speed and **b)** angular acceleration of beam

kept constant no matter either ω_0 or T is increased or vice versa. However, this is not the case because the geometric stiffness changes proportional to ω_0 squared, which can be observed in the plots given below. That both effects, i.e. the angular acceleration and the geometric stiffness, are determinant for elastic displacements should always be accounted for.

To generalize the results of analysis the equations of motion were made non-dimensional by dividing elastic displacements u, v and s by the length of beam L, and multiplying the real time t by $\omega^* = \frac{1}{L^2}\left(\frac{EI}{\rho A}\right)^{1/2}$ so that the dimensionless coordinate and displacements are now x/L, u/L, v/L, s/L as the non-dimensional time τ is than $\tau = \omega^* t$. Note that the slope of elastic curve does not alter according to these new definitions.

In order to investigate the effects of ω_0 and T, one of these parameters was changed, as the other was held constant. Both parameters were replaced their non-dimensional counterparts ω_0^* and T^* so that $\omega_0^* = \omega_0/\omega^*$ and $T^* = \omega^* T$. The first bending frequency of non-rotating cantilever is $\omega_I = (1.875)^2\ \omega^* \cong 3.51\omega^*$, thus the non-dimensional first frequency $\omega_I^* = \omega_I/\omega^* = 3.51$. To compare the dynamic models described above, three different values for ω^* were chosen:

$$\omega_0^* = 0.35 = \frac{1}{10}\omega_I^*, \quad \omega_0^* = 3.51 = \omega_I^* \quad \text{and} \quad \omega_0^* = 7 = 2\omega_I^*.$$

These values correspond to one tenth of, itself and twice the first bending frequency. The values selected for T^* were 8.1, 16.2 and 32.4 to compare the results with those given in [14]. Using the physical parameters given in that paper one obtains $\omega^* = 1.08$. When T^* values are divided by $\omega^* = 1.08$ their counterparts in actual time scale are found as $T = 7.5$, 15 and 30 seconds. Note that ω_0^* values chosen are lower than second non-dimensional bending frequency $\omega_{II}^* \cong 22$.

The plotted curves can be qualitatively compared with each other in two ways since there are two parameters, i.e. ω_0^* and T^*. For instance, keeping T^* constant, it can be evaluated how the order of ω^* affects the results and vice versa. In Figures 3 to 5, the

deflection curves of tip point corresponding to ω_0^*=0.35; 3.51 and 7 are plotted for the fixed value of T^*=32.4. If one assumes the maximum normal force due to rotation as 1 unit for ω_0^*=3.51, it will be hundred times less than this when ω_0^*=0.35, and four times larger when ω_0^*=7. At a speed of as low as 0.35 all the models, especially the SVM and VNM, give almost the same results for transversal deflections, Figure 3a. However, longitudinal displacements remarkably differ from each other as shown in Figure 3b.

In fact, the UVM is expected to give smaller displacements relative to the SVM for the reasons explained previously. The difference among three models begins to be more obvious when ω_0^*=3.51, Figure 4a. The curves in Figure 5a also follow the same pattern.

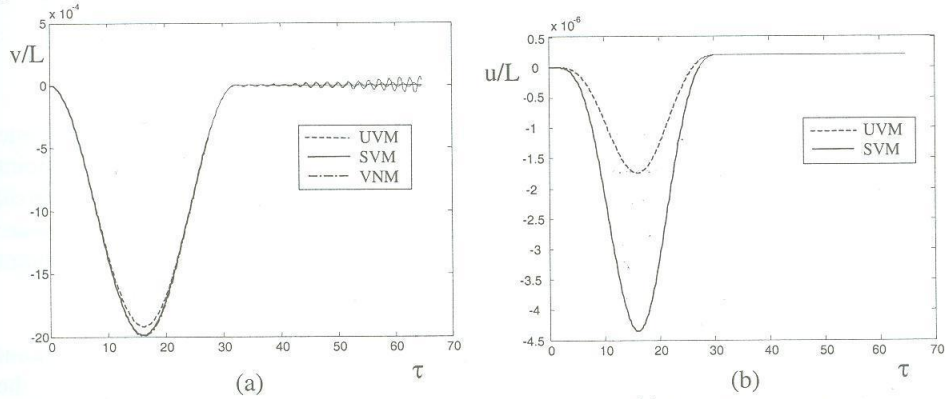

Figure 3. Non-dimensional a) transversal deflections and b) longitudinal deflections of the tip point found by different models for ω_0^*=0.35, T^*=32.4.

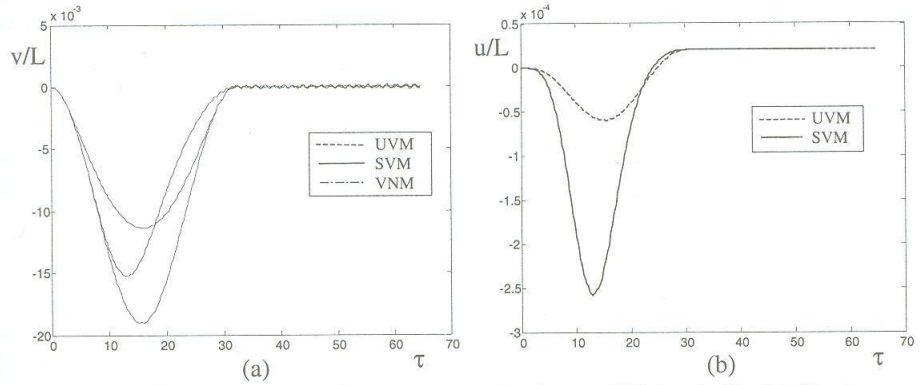

Figure 4. Non-dimensional a) transversal deflections and b) longitudinal deflections of the tip point found by different models for ω_0^*=3.51, T^*=32.4.

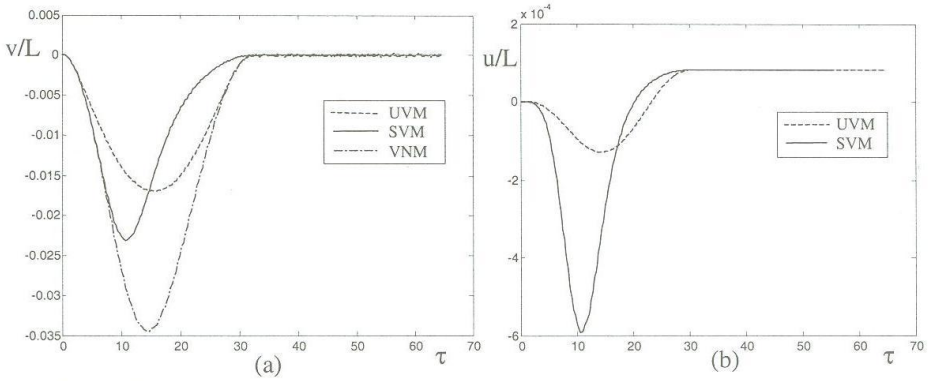

Figure 5. Non-dimensional a) transversal deflections and b) longitudinal deflections of the tip point found by different models for ω_0^*=7, T^*=32.4.

Another notable point is that the transversal deflection curves of the SVM become asymmetric over the time span T^* while the VNM given the maximum tip point displacement nearly always at $\tau=T^*/2$. The reason for this is that the effect of transversal displacement on the normal force is not included in the VNM. The u-displacements are also plotted in Figure 4b and 5b. As expected, the longitudinal displacement of tip point is always smaller than that obtained by the SVM.

In Figures 6 to 8 the similar curves for T^*=16.2 are presented. For ω_0^*=0.35 the tip point deflection curves obtained by the SVM and VNM are nearly coincident. However, the curve of the UVM goes away from the others in comparison with the curves for T^*=32.4 because the angular acceleration gets larger as T^* becomes smaller. The asymmetry of the curves by the SVM is observed in these figures as well. Finally, Figures 9 to 11 show the curves for T^*=8.1. It can be clearly seen in these figures that the curves separate from each other considerably.

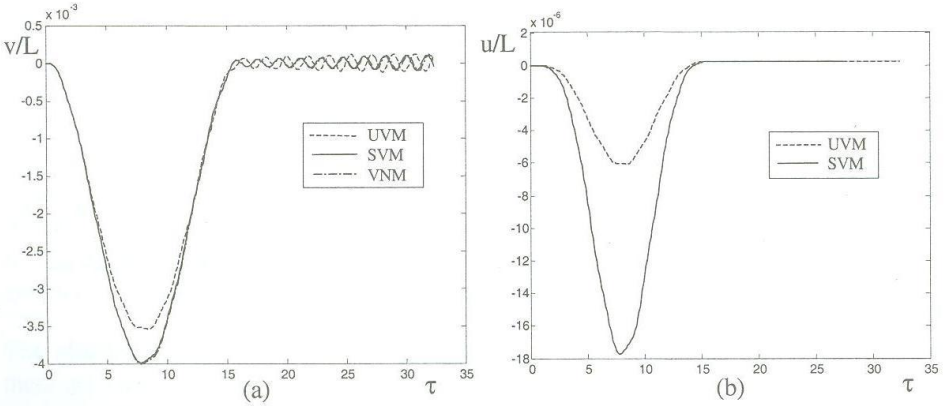

Figure 6. Non-dimensional a) transversal deflections and b) longitudinal deflections of the tip point found by different models for ω_0^*=0.35, T^*=16.2.

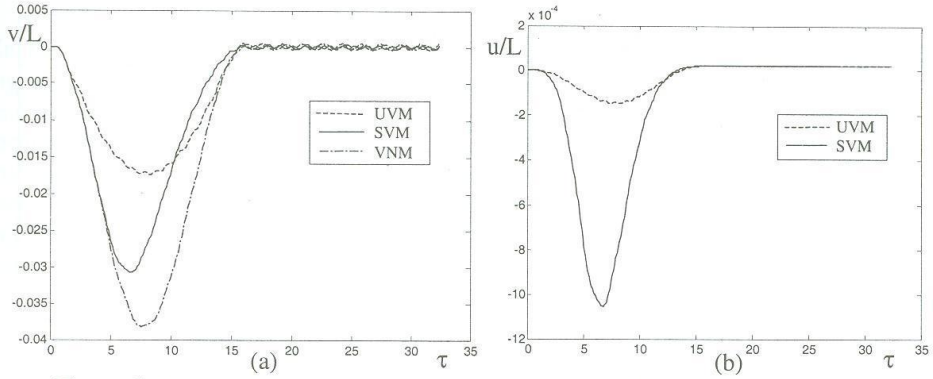

Figure 7. Non-dimensional a) transversal deflections and b) longitudinal deflections of the tip point found by different models for $\omega_0^*=3.51$, $T^*=16.2$.

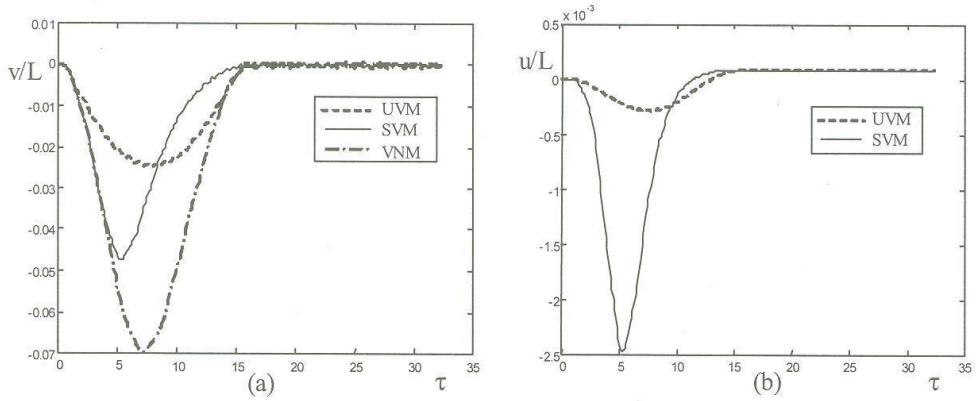

Figure 8. Non-dimensional a) transversal deflections and b) longitudinal deflections of the tip point found by different models for $\omega_0^*=7$, $T^*=16.2$.

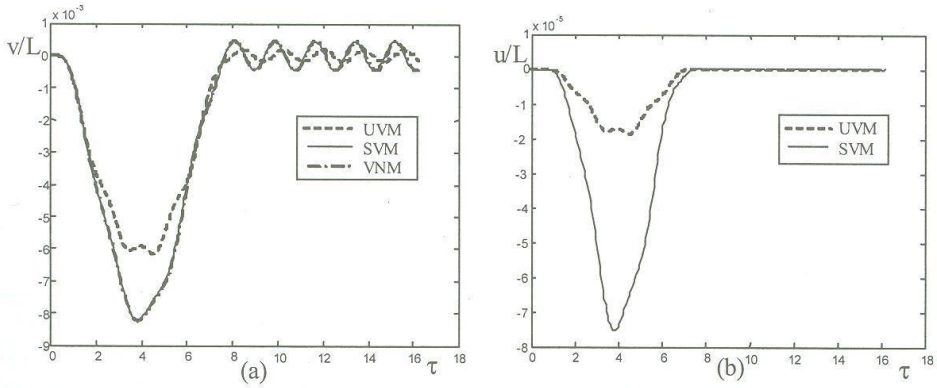

Figure 9. Non-dimensional a) transversal deflections and b) longitudinal deflections of the tip point found by different models for $\omega_0^*=0.35$, $T^*=8.1$.

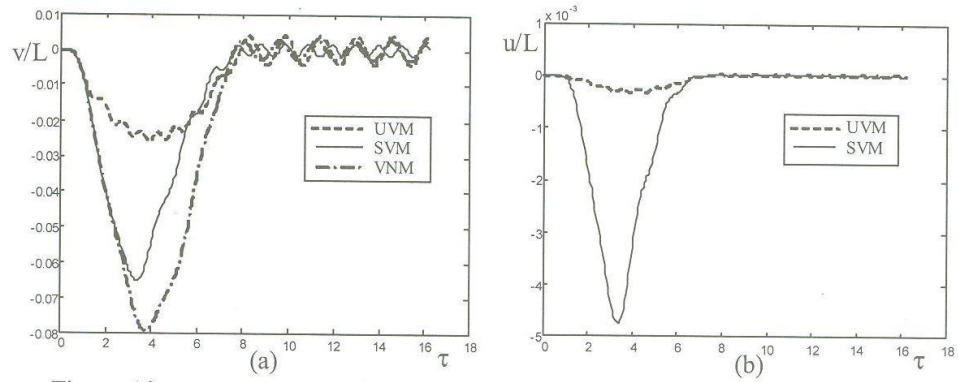

Figure 10. Non-dimensional a) transversal deflections and b) longitudinal deflections of the tip point found by different models for ω_0^*=3.51, T^*=8.1.

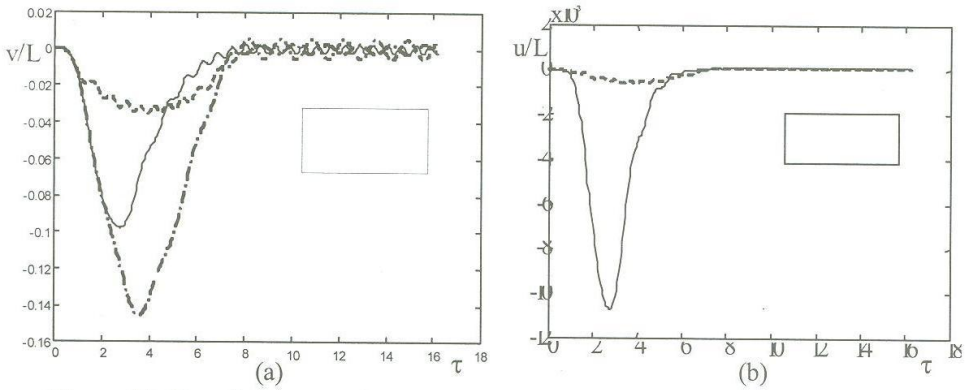

Figure 11. Non-dimensional a) transversal deflections and b) longitudinal deflections of the tip point found by different models for ω_0^*=7, T^*=8.1.

In addition to the qualitative examination made so far, to enable one also a numerical evaluation of the results the tip point deflections obtained from each model are summarized in Table 1 provided that the deflection by the SVM is assumed as 1 unit (or hundred percent).

Table 1. Tip point deflections found by each model with respect to different ω_0^* and T^* values for cycloidal angular speed program
(All deflection values are divided by that of the SVM)

T^*	$32.4=30\omega^*$			$16.2=15\omega^*$			$8.1=7.5\omega^*$		
Models / ω_0^*	UVM	SVM	VNM	UVM	SVM	VNM	UVM	SVM	VNM
$0.35=0.1\omega_I^*$	0.950	1.000	1.000	0.875	1.000	1.000	0.756	1.000	1.000
$3.5=\omega_I^*$	0.745	1.000	1.241	0.568	1.000	1.240	0.400	1.000	1.217
$7=2\omega_I^*$	0.735	1.000	1.493	0.526	1.000	1.479	0.363	1.000	1.485

In Table 1, the values obtained from the SVφM do not appear because they are in full agreement with those of the SVM, which is caused by choosing a very large slenderness ratio, i.e. L/i where i is the gyration radius of cross-sectional area, and L is the length of beam. For example, in [14], this ratio is about 447. The reason for taking such a value for slenderness in the computations is to make a comparison between the results found here and in [14]. However, to examine when shear effect becomes dominant another analysis was carried out using the dimensional physical parameters. It is observed that the relative error defined by

$$\frac{\textit{deflection by the } \text{SV}\varphi\text{M} - \textit{deflection by the } \text{SVM}}{\textit{deflection by the } \text{SV}\varphi\text{M}} \times 100$$

varies from 2% to 14% while the slenderness ratio is decreased from 20 to 4. For a beam with solid circular cross-section a slenderness equal to 20 means $L=5D$ where D is cross-sectional diameter of beam. As a consequence, for beam with L/i >20, the SVM is quite reliable model.

As visualization of Table 1, Figure 12 shows how the tip point deflections found by each model vary with respect to different ω_0^* and T^* values in surface plots.

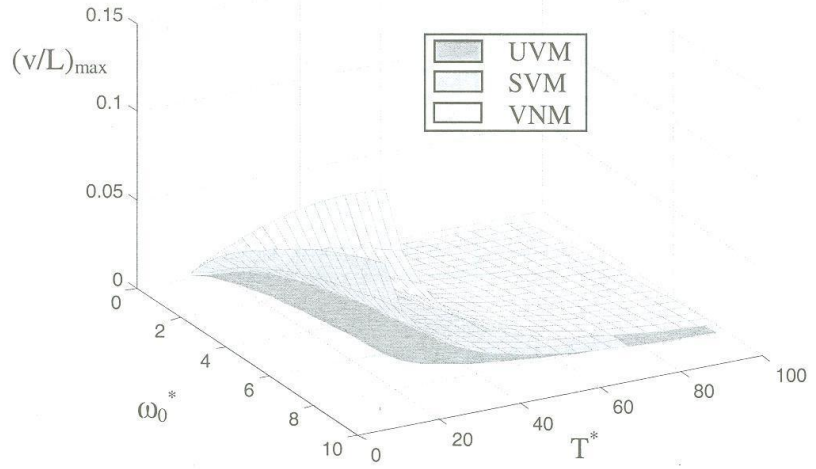

Figure 12. Non-dimensional tip point deflections found by each model with respect to different ω_0^* and T^* values in surface plots

The analysis has been repeated by using another motion program for angular velocity to examine how to affect the overall dynamic behaviour of beam. To this end, a parabolic law defined below was used:

$$\begin{aligned} \omega &= 2\omega_0\left(\frac{t}{T}\right)^2 && 0\le t\le T/2 \\ \omega &= \omega_0\left[-2\left(\frac{t}{T}\right)^2+4\left(\frac{t}{T}\right)-1\right] && T/2<t\le T \\ \omega &= \omega_0 && t>T \end{aligned} \tag{19}$$

from which the following relationship for angular acceleration is obtained:

$$\begin{aligned} \alpha &= \frac{4\omega_0}{T^2}t && 0 \le t \le T/2 \\ \alpha &= \frac{4\omega_0}{T^2}(T-t) && T/2 < t \le T \\ \alpha &= 0 && t > T \end{aligned} \tag{20}$$

The maximum value of angular velocity is $2\omega_0/T$, so the same as the cycloidal program has. Although the results are not presented as figures here due to limited space, they are given in Table 2 similar to Table 1. The results have same tendency as in the case of cycloidal speed function, that is, the UVM gives smaller deflections and the VNM produces bigger deflections in comparison with those obtained from the SVM.

Table 2. Tip point deflections found by each model with respect to different ω_0^* and T^* values for parabolic angular speed program
(All deflection values are divided by that of the SVM)

T^*	$32.4=30\omega^*$			$16.2=15\omega^*$			$8.1=7.5\omega^*$		
Models / ω_0^*	UVM	SVM	VNM	UVM	SVM	VNM	UVM	SVM	VNM
$0.35=0.1\omega_I^*$	0.950	1.000	1.000	0.880	1.000	1.000	0.817	1.000	1.000
$3.5=\omega_I^*$	0.833	1.000	1.362	0.640	1.000	1.416	0.448	1.000	1.314
$7=2\omega_I^*$	0.873	1.000	1.676	0.629	1.000	1.692	0.425	1.000	1.531

Finally, the results obtained by the models studied in this paper, based on input data in [14] and those given in [14] will be presented for the purpose of comparison. Also in [14], the Euler-Newtonian equations of motion are derived. These equations are solved by using the finite element method along with the Galerkin procedure. Any information about the interpolation functions is not given but it is strongly possible that the usual Hermite polynomials were employed. To remove the non-linear coupling between the equations for u and v due to the axial force, the authors of [14] replaced it with the centrifugal force for the case of a rigid beam. The graphics in [14], which for the longitudinal u, the transversal v deflection and the slopes φ of the tip point, are repeated in Figure 13a, b and c.

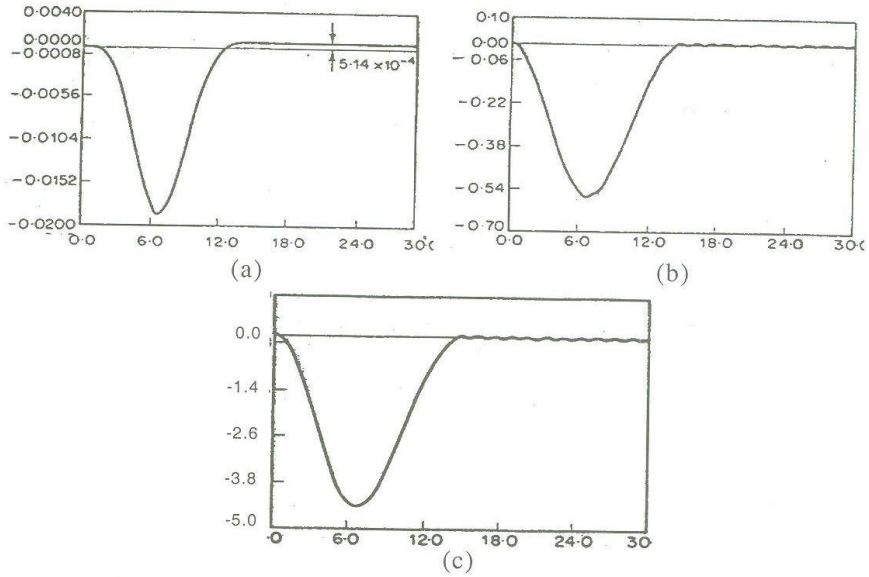

Figure 13. Longitudinal deflection (a), transversal deflection (b) and slopes (c) of the tip point given in [14]. The horizontal axis shows time.

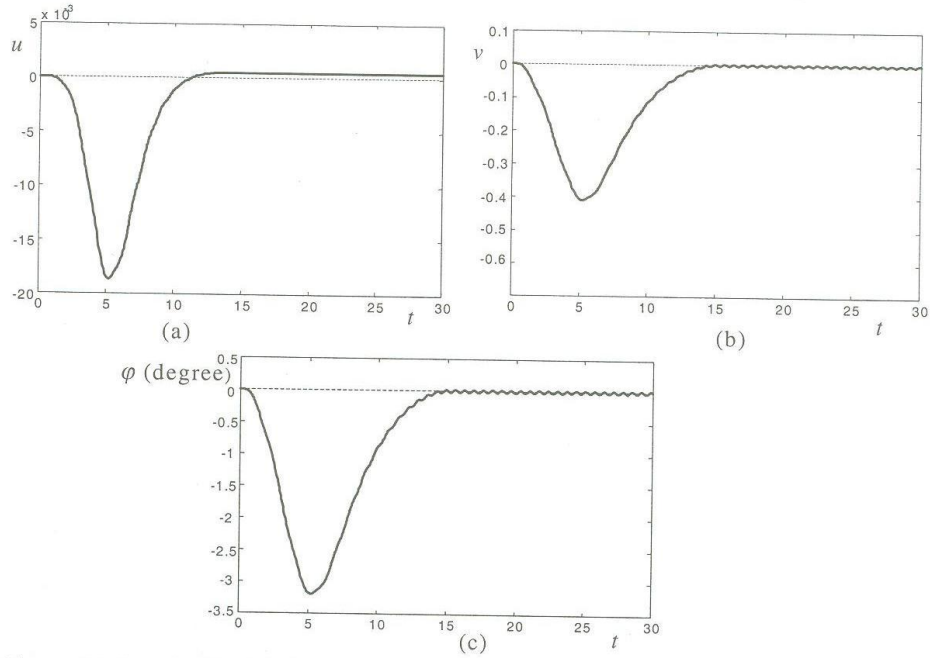

Figure 14. Longitudinal deflections (a), transversal deflections (b), and slopes (c) of the tip point found from the SVφM (based on the input data given in [14]).

Figure 14 shows the results obtained from the SVφM. From the comparison of these figures with Figure 13, it is clear that the maximum values of v and φ do not coincide but are of the same order. The reason for this was explained above. This is a different approach that leads to a model representing a transition from the VNM to the UVM.

4. CONCLUSIONS

In this paper, four dynamic models that have been used in many papers on rotating flexible beams were presented and examined. One can summarize some basic conclusions drawn from this study as follows:
In comparison with the SVM, the UVM gives relatively small values for both transversal and longitudinal deflections. In contrast, the VNM yields larger values then the SVM. In the UVM and in the SVM, the same spatial functions for u and s, respectively, were used. These functions are the eigenmodes of a fixed-free, longitudinally vibrating rod. It is obvious that the u-displacements are forced to satisfy the boundary condition $EA\frac{\partial u}{\partial x}(L,t)=0$ at free end of beam while in fact this is not the case. In other words, the system is subject to mathematical constraints if not physically. Thus, the system apparently becomes stiffer and the deflections get smaller. To compensate this principal error, an algebraic constrain must be introduced for free end of beam using equation (3) as Ryan et al did in [9].

The VNM is quite simple model, but it does not consider the interaction between transversal deflections and centrifugal force. The SVM appears to be the most reliable model, because it is consistent with physical conditions under which the beam operates. At high speeds, the VNM can be evaluated as a prudential model.

5. REFERENCES

[1] H. Du, M.K. Lim, K.M. Liew, A Nonlinear Finite Element Model For Dynamics of Flexible Manipulators, Mechanism and Machine Theory **31(8)**, 1109-1119, 1996.
[2] V. Feliu, K.S. Rattan, H.B. Brown, Modeling and Control of Single-Link Flexible Arms With Lumped Masses, ASME Journal of Dynamic Systems, Measurements, and Control **114**, 59-69, 1992
[3] W.D. Zhu, C.D. Mote, Dynamic Modeling and Optimal Control of Rotating Euler-Bernoulli Beams, ASME Journal of Dynamic Systems, Measurements, and Control **119**, 802-808, 1997
[4] H. Diken, Vibration Control of A Rotating Euler-Bernoulli Beam, Journal of Sound and Vibration **232(3)**, 541-551, 2000
[5] S. Telli, Analysis of Dynamic Behaviour of a Manipulator With Flexible Link, Ph.D. Dissertation, Uludag University (in Turkish). 2000.
[6] A. Yiğit, R.A. Scott, A.G. Ulsoy, Flexural Motion of a Radially Rotating Beam Attached to a Rigid Body, Journal of Sound and Vibration **121(2)**, 201-210, 1988
[7] F.L. Hu, A.G. Ulsoy, Dynamic Modelling of Constrained Flexible Robot Arms for Controller Design, ASME Journal of Dynamic Systems, Measurements, and Control **116**, 56-65, 1994
[8] S. Hanagud, S. Sarkar, Problem of the Dynamic's of a Cantilever Beam Attached

to a Moving Base, J.Guidance **12(3)**, 438, 1989

[9] W.J. Haering, R.R. Ryan, R.A. Scott, New Formulation for Flexible Beams Undergoing Large Overall Motion, J.Guidance, Control, and Dynamics **17(1)**, 76-83, 1994

[10] H.H. Yoo, R.R. Ryan, R.A. Scott, Dynamics of Flexible Beams Undergoing Overall Motion, Journal of Sound and Vibration **181(2)**, 261-278, 1995

[11] W.H. Haering, Simple Flexible-Body Dynamic Beam Formulations: Deformation Choices, Boundary Conditions and Strain Approximations, 42nd AIAA/ASME/ ASCE/AHS/ASC Structures, Structural Dynamics and Materials Conference and Exhibit, Seattle, WA, USA, April 2001

[12] T.R. Kane, R.R. Ryan, Dynamics of a Cantilever Beam Attached to a Moving Base, Journal of Guidance **10(2)**, 139-151, 1987

[13] S. Choura, S. Jayasuriya, M.A. Medick, On the Modelling, and Open-Loop Control of a Rotating Thin Flexible Beam, ASME Journal of Dynamic Systems, Measurements, and Control **113**, 26-33, 1991

[14] J.C. Simo, L.Vu-Quoc, The Role of Non-linear Theories In Transient Dynamic Analysis of Flexible Structures, Journal of Sound and Vibration **119(3)**, 487-508, 1987